IMU Shoulder Angle Estimation: Effects of Sensor-to-Segment Misalignment and Sensor Orientation Error

Kezhe Zhu, Jinxuan Li, Dongxuan Li, Bingfei Fan, and Peter B. Shull, *Member, IEEE*

***Abstract*— Accurate shoulder joint angle estimation is crucial for analyzing joint kinematics and kinetics across a spectrum of movement applications including in athletic performance evaluation, injury prevention, and rehabilitation. However, accurate IMU-based shoulder angle estimation is challenging and the specific influence of key error factors on shoulder angle estimation is unclear. We thus propose an analytical model based on quaternions and rotation vectors that decouples and quantifies the effects of two key error factors, namely sensor-to-segment misalignment and sensor orientation estimation error, on shoulder joint rotation error. To validate this model, we conducted experiments involving twenty-five subjects who performed five activities: yoga, golf, swimming, dance, and badminton. Results showed that improving sensor-to-segment misalignment along the segment's extension/flexion dimension had the most significant impact in reducing the magnitude of shoulder joint rotation error. Specifically, a 1° improvement in thorax and upper arm calibration resulted in a reduction of 0.40° and 0.57° in error magnitude. In comparison, improving IMU heading estimation was only roughly half as effective (0.23° per 1°). This study clarifies the relationship between shoulder angle estimation error and its contributing factors, and identifies effective strategies for improving these error factors. These findings have significant implications for enhancing the accuracy of IMU-based shoulder angle estimation, thereby facilitating advancements in IMU-based upper limb rehabilitation, human-machine interaction, and athletic performance evaluation.**

***Index Terms*— Inertial sensors, orientation estimation, sensor-to-segment alignment, shoulder angle estimation.**

Manuscript received 9 August 2023; revised 26 October 2023; accepted 4 November 2023. Date of publication 8 November 2023; date of current version 14 November 2023. This work was supported by the National Natural Science Foundation of China under Grant 52250610217. *(Corresponding author: Peter B. Shull.)*

This work involved human subjects or animals in its research. Approval of all ethical and experimental procedures and protocols was granted by the Ethics Committee of Shanghai Jiao Tong University under Application No. E2021013P, and performed in line with the Helsinki Declaration.

Kezhe Zhu, Jinxuan Li, Dongxuan Li, and Peter B. Shull are with the State Key Laboratory of Mechanical System and Vibration, School of Mechanical Engineering, Shanghai Jiao Tong University, Shanghai 200240, China (e-mail: kezhe_zhu@sjtu.edu.cn; jinxli@sjtu.edu.cn; sjtu_dongxuanli@sjtu.edu.cn; pshull@sjtu.edu.cn).

Bingfei Fan is with the College of Mechanical Engineering, Zhejiang University of Technology, Hangzhou 310014, China (e-mail: bingfeifan@zjut.edu.cn).

Digital Object Identifier 10.1109/TNSRE.2023.3331238

I. Introduction

THE shoulder joint plays a vital role in daily life and sports [1], [2], [3], requiring accurate and portable angle estimation for applications such as home-based rehabilitation [4], human-machine interaction [5], and sports performance evaluation in real-world environments [6], [7], [8]. In this regard, the utilization of an inertial motion capture (IMC) system, consisting of inertial measurement units (IMUs), presents a low-cost and portable solution for upper limb motion capture [9], [10].

Numerous methods have been developed to estimate shoulder joint rotation or angles [11], [12], [13], [14], [15], [16], [17], but the accuracy of these estimations can vary depending on factors such as the experimental environment, motion velocity, and sensor positioning [18]. However, the estimation error can be attributed to two key factors: IMU orientation estimation error and sensor-to-segment misalignment [19], [20]. IMU orientation estimation tracks the movement of the segment, while sensor-to-segment alignment ensures that the estimated IMU local coordinate system aligns with the segment's anatomical coordinate system. Consequently, the joint rotation is determined as the relative orientation between two adjacent segments [21], which are tracked by sensors attached to them. Joint angles can be obtained by applying Euler decomposition to the joint rotation if required. Therefore, the aforementioned primary error sources can be categorized as the underlying factors contributing to the key error factors, which can be quantified through experiments.

Despite the categorization of error sources into sensor-to-segment misalignment and IMU orientation estimation error, the effects of these two key factors on shoulder rotation errors remain unclear. This knowledge gap hinders the development of shoulder angle estimation-related applications and the improvement of accuracy in such systems. Sensor-to-segment alignment methods, also known as calibration, have been extensively studied and validated for their accuracy and repeatability in previous research [20], [22], [23]. Additionally, the estimation errors of IMU orientation and shoulder joint angle during sports and rehabilitation movements have been widely documented [20], [24]. However, limited research has investigated the effects of these error factors on joint rotation or angles. Fan et al. [19] analyzed the effects of sensor-to-segment misalignment and IMU orientation errors on knee

angles during drop landing and cutting trials. However, these effects were computed by simulating each error factors at various levels, lacking quantitative evidence of the impact of these factors on joint angle estimation accuracy. Importantly, none of these studies have performed a direct analytical assessment of the error factor changes on the improvement of joint angle estimation accuracy. As a result, existing research on error factors cannot offer analytical guidance or implications for applications involving shoulder angle estimation. While studies reporting shoulder joint errors under varying circumstances offer limited instruction for novel research due to the variability in experimental environments and protocol requirements. Consequently, the absence of a model connecting error factors and joint rotation errors hinders the impact of research dedicated to error factors and the advancements in shoulder angle estimation accuracy.

Previous research suggested that improving calibration methods or IMU orientation estimation can help reduce joint angle estimation error [25], [26], [27], [28]. However, none have provided analytical models to assess the effectiveness of these potential error reduction methods, resulting in a lack of specific guidelines for improving estimation accuracy in their specific applications based on collected data. In addition to deriving guidance from calibration or IMU orientation estimation validation for joint angle estimation, it is also crucial to obtain instructions from existing experimental results backwards to effectively reduce these two key error factors and improve estimation accuracy. Therefore, the comprehensive model connecting the error factors and the joint angle estimation error should also identify the specific error factor components that have the greatest impact on reducing the estimation error, taking the research a step further.

In this paper, we present a novel model to decouple and analytically quantify the effects of key error factors on shoulder angle estimation in two steps. Specifically, our model connects the IMU-based shoulder angle estimation error, expressed as joint rotation error in rotation vector, with two key error factors: sensor-to-segment misalignment and IMU orientation estimation error, both represented by rotation vectors. First, a linear approximation model on quaternions and rotation vectors is proposed to bridge the gap between shoulder rotation error and its underlying key error factors. Second, by leveraging this approximation model, we analytically derive the "effect Jacobian" of these key error factors, which quantitatively measures the impact of each factor component's improvement on the overall estimation accuracy by partial derivative. To validate the proposed model, we conducted an experiment involving five different activities. The results have provided valuable insights into the impact of reducing specific error factor components on the improvement of shoulder angle estimation accuracy. Through the quantification of these effects, we aim to identify the significant components and determine the appropriate adjustment strategies for enhancing estimation accuracy, based on the existing experimental results.

To the best of our knowledge, this study is the first to present a direct analytical model connecting joint angle estimation error with its error sources. Additionally, it is the first study to provide a quantified assessment of the significance of each error factor component on reducing joint rotation error, based on the obtained experimental results. Our work could have important implications for the development of calibration methods and IMU orientation estimation techniques, as it converts their progress into valuable guidance for improving the accuracy of inertial motion capture systems. By offering insights into the significance of error factor components based on specific experimental data, our study could also contribute to the implementation and advancement of accurate rehabilitation and sports performance evaluation systems tailored to individuals or activities.

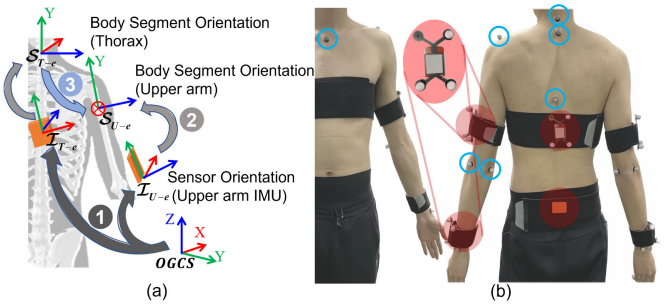

Fig. 1. Procedure and experimental setup for shoulder joint angle estimation. (a) The shoulder joint angle estimation algorithm consists of three steps. 1) sensor orientation estimation: Determines the orientation of the sensor with respect to the inertial-global reference coordinate system; 2) sensor-to-segment alignment: Obtains the alignment transformations between the sensors and the segment coordinate system through calibration; 3) shoulder rotation/angle calculation: Computes the relative orientation between the proximal segment (thorax) and the distal segment (upper arm) as the shoulder rotation and further decomposes it into shoulder angles. (b) The experiment utilizes OMC with nine markers on each side of the upper limb and seven markers on the thorax to define and track the body segment coordinate system.

II. Methods

A. IMU-Based Shoulder Angle Estimation

Consistent with the CAST procedure [29] employed in OMC, shoulder joint rotation is estimated by IMC following the three-step procedure [13], [30] (Fig. 1), where the shoulder joint rotation is defined as the relative orientation between the proximal segment (thorax) and distal segment (upper arm) [21], as described by

$$ {}_{JA-e}\boldsymbol{q} = \left({}^{OGCS}\boldsymbol{q}_{\mathcal{S}_{T-e}}\right)^{*} \otimes {}^{OGCS}\boldsymbol{q}_{\mathcal{S}_{U-e}} \tag{1} $$

where ${}^{OGCS}\boldsymbol{q}_{\mathcal{S}_{T-e}}$ and ${}^{OGCS}\boldsymbol{q}_{\mathcal{S}_{U-e}}$ represent the orientation quaternions of the body segment ($\mathcal{S}$), thorax (T), and upper arm (U) coordinate systems (CS), as estimated by the IMC. ${}_{JA-e}\boldsymbol{q}$ denotes the IMC-estimated shoulder joint rotation, which can be further decomposed into shoulder Euler angles.

The math denotations of the CSs, rotation and errors are summarized in Table I. The body segment movement is tracked by the adhering IMU assuming that the invariant sensor-to-segment alignment transformation throughout the trial. This sensor-to-segment alignment transformation can be obtained by various calibration methods such as static calibration [22], [30] and functional calibration [13], [31], [32]. Therefore, the segment CS orientation with respect to the

TABLE I
MATHEMATICAL NOTATIONS AND EXPLANATIONS

Type	Denotation	Representation
CS	$\mathcal{S}_{\forall-r/e}$	Reference/Estimated segment CS
CS	$\mathcal{I}_{\forall-r/e}$	Reference/Estimated IMU local CS on segment $\forall$
CS	$\mathcal{T}_{\forall-r}$	Reference marker cluster local CS on segment $\forall$
Rotation	${}^{\mathcal{A}}\boldsymbol{q}^{t}_{\mathcal{B}}$	Rotation quaternion from CS $\mathcal{A}$ to $\mathcal{B}$ at time t
Rotation	${}^{\mathcal{A}}\boldsymbol{\phi}^{t}_{\mathcal{B}}$	Rotation vector from CS $\mathcal{A}$ to $\mathcal{B}$ at time t
Rotation	${}^{\mathcal{A}}\boldsymbol{R}_{\mathcal{B}}$	Rotation matrix from CS $\mathcal{A}$ to $\mathcal{B}$
Error	$Calib_{\forall}\boldsymbol{\delta q}$	Calibration error quaternion of segment $\forall$
Error	$OriEst_{\forall}\boldsymbol{\delta q}^{t}$	Sensor orientation estimation error quaternion of segment $\forall$ at time t
Error	$Calib_{\forall}\boldsymbol{\delta\phi}$	Calibration error rotation vector of segment $\forall$
Error	$OriEst_{\forall}\boldsymbol{\delta\phi}^{t}$	Sensor orientation estimation error rotation vector of segment $\forall$ at time t

The any 'segment $\forall$' could be thorax T or upper arm U in shoulder joint rotation calculation. (CS: Coordinate system; OGCS: Global CS defined by Optical motion capture system; IGCS: Global CS defined by Inertial motion capture system)

optical-global reference CS ($OGCS$) is estimated from IMU orientation and sensor-to-segment alignment transformation as follows,

$$ {}^{OGCS}\boldsymbol{q}^{t}_{\mathcal{S}_{\forall-e}} = {}^{OGCS}\boldsymbol{q}_{IGCS} \otimes {}^{IGCS}\boldsymbol{q}_{\mathcal{I}_{\forall-e}} \otimes {}^{\mathcal{I}_{\forall-e}}\boldsymbol{q}_{\mathcal{S}_{\forall-e}} \quad (2) $$

where ${}^{IGCS}\boldsymbol{q}_{I_{\forall-e}}$ denotes orientation of the estimated IMU local CS $\mathcal{I}_{\forall-e}$ on a body segment (thorax or upper arm) with respect to inertial-global reference CS ($IGCS$), ${}^{\mathcal{I}_{\forall-e}}\boldsymbol{q}_{\mathcal{S}_{\forall-e}}$ denotes the sensor-to-segment alignment transformation quaternion of a body segment and ${}^{OGCS}\boldsymbol{q}_{IGCS}$ denotes the transformation aligning OGCS and IGCS, which is obtained by methods introduced in [33] and [34]. The quaternion representation of the shoulder joint rotation is obtained by substituting (2) into (1). When specifically focusing on the estimation of shoulder joint rotation while disregarding joint translation, it becomes evident that various error factors, including calibration methods, experimental environment, and motion velocity, can be consolidated into two key error factors (Fig. 2): sensor-to-segment alignment error and sensor orientation estimation error. Two key error factors associated with each segment subsequently contribute to the overall shoulder rotation error.

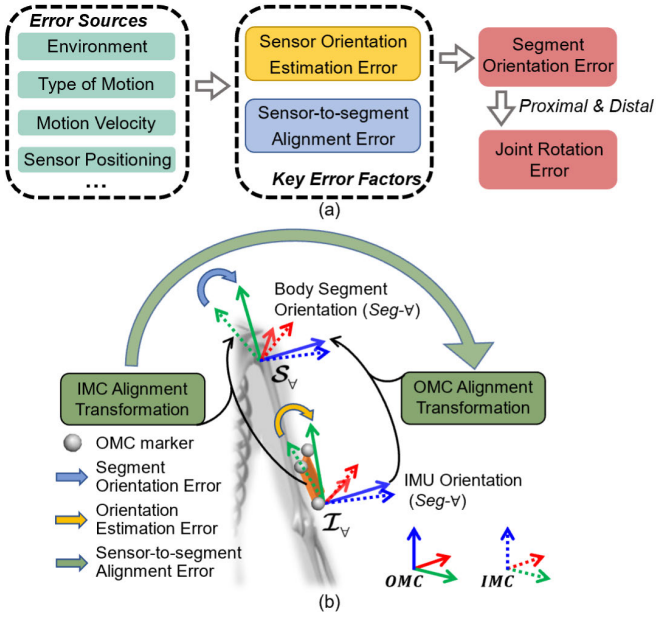

Fig. 2. Demonstration of analyzed errors. (a) Interrelationship of analyzed errors. (b) Illustration of segment orientation error, sensor-to-segment misalignment, and orientation estimation error at a random pose.

1) Sensor-to-Segment Alignment Error: The sensor-to-segment alignment error $Calib_{\forall}\boldsymbol{\delta q}$ of each segment is defined as the relative transformation between the reference and estimated sensor-to-segment alignment transformation, formulated as follows,

$$ Calib_{\forall}\boldsymbol{\delta q} = \left({}^{\mathcal{I}_{\forall-e}}\boldsymbol{q}_{\mathcal{S}_{\forall-e}}\right)^{*} \otimes {}^{\mathcal{I}_{\forall-r}}\boldsymbol{q}_{\mathcal{S}_{\forall-r}} \quad (3) $$

where ${}^{\mathcal{I}_{\forall-e}}\boldsymbol{q}_{\mathcal{S}_{\forall-e}}$ and ${}^{\mathcal{I}_{\forall-r}}\boldsymbol{q}_{\mathcal{S}_{\forall-r}}$ denote the estimated and reference sensor-to-segment alignment transformation for a segment, respectively. The reference sensor-to-segment alignment refers to the transformation between OMC segment CS and reference IMU local CS, which is derived from the reference marker cluster local CS.

2) Sensor Orientation Estimation Error: Multiple algorithms have been developed to estimate the IMU orientation, but it is important to note that the these algorithms estimate the orientation with respect to the IGCS of each IMU. These IGCSs typically differ from the OGCS and the IGCSs of other IMUs [35]. Consequently, OGCS and IGCS of each IMU require an independent alignment process [33], [34]. The sensor orientation estimation error at time t is quantified as the relative orientation between the estimated and reference sensor orientation expressed in $OGCS$ [26], formulated as follows,

$$ \begin{aligned} OriEst\boldsymbol{\delta q}^{t} &= {}^{OGCS}\boldsymbol{q}^{t}_{\mathcal{I}_{\forall-r}} \otimes \left({}^{OGCS}\boldsymbol{q}^{t}_{\mathcal{I}_{\forall-e}}\right)^{*} \\ &= {}^{OGCS}\boldsymbol{q}^{t}_{\mathcal{I}_{\forall-r}} \otimes \left({}^{OGCS}\boldsymbol{q}_{IGCS} \otimes {}^{IGCS}\boldsymbol{q}_{\mathcal{I}_{\forall-e}}\right)^{*} \end{aligned} \quad (4) $$

B. Shoulder Rotation Error Linear Approximation

Joint rotation calculations could interconnect error components from various sources and segments, resulting in a complex and non-intuitive relationship. Therefore, the shoulder rotation error is first linearly approximated as the

composition of error vectors in this section, and then the partial derivative of the approximated shoulder rotation error magnitude with respect to the XYZ components of the key error factors is introduced in section II-C.

Joint angles are usually expressed in Euler angle due to its concise physical interpretation. However, Euler angles suffer from the gimbal lock problem, which occurs in T-pose following the anatomical segment CS definition recommended by ISB [21]. Therefore, in this paper, joints and joint errors are represented by joint rotations using quaternions instead of joint angles, as the former are immune to gimbal lock issues and can be transformed into joint angles when required. Joint rotation error, which comprises the sensor-to-segment alignment error and sensor orientation estimation error defined above, is defined as the relative quaternion between the reference joint rotation quaternion and the estimated joint rotation, and is formulated as follows,

$$\begin{aligned} {}_{JA}\boldsymbol{\delta q} &= ({}_{JA-r}\boldsymbol{q})^* \otimes {}_{JA-e}\boldsymbol{q} \\ &= \left({}^{\mathcal{S}_{T-r}}\boldsymbol{q}_{\mathcal{S}_{U-r}}\right)^* \otimes {}^{\mathcal{S}_{T-e}}\boldsymbol{q}_{\mathcal{S}_{U-e}} \end{aligned} \tag{5}$$

The relationship between the estimated and reference shoulder rotation is derived by introducing orientation errors of segment CS and extending (1), as follows,

$$\begin{aligned} {}_{JA-e}\boldsymbol{q}^t &= \left({}^{OGCS}\boldsymbol{q}^t_{\mathcal{S}_{T-r}} \otimes \left({}^{\mathcal{S}_{T-e}}\boldsymbol{\delta q}^t_{\mathcal{S}_{T-r}}\right)^*\right)^* \\ &\quad \otimes {}^{OGCS}\boldsymbol{q}^t_{\mathcal{S}_{U-r}} \otimes \left({}^{\mathcal{S}_{U-e}}\boldsymbol{\delta q}^t_{\mathcal{S}_{U-r}}\right)^* \\ &= {}^{\mathcal{S}_{T-e}}\boldsymbol{\delta q}^t_{\mathcal{S}_{T-r}} \otimes {}_{JA-r}\boldsymbol{q}^t \otimes \left({}^{\mathcal{S}_{U-e}}\boldsymbol{\delta q}^t_{\mathcal{S}_{U-r}}\right)^* \end{aligned} \tag{6}$$

where ${}^{\mathcal{S}_{T-e}}\boldsymbol{\delta q}^t_{\mathcal{S}_{T-r}}$ and ${}^{\mathcal{S}_{U-e}}\boldsymbol{\delta q}^t_{\mathcal{S}_{U-r}}$ denotes the orientation error between estimated and reference segment CS of thorax and upper arm, respectively. The segment orientation error can be derived as follows,

$$\begin{aligned} &{}^{\mathcal{S}_{\forall-e}}\boldsymbol{\delta q}^t_{\mathcal{S}_{\forall-r}} \\ &= \left({}^{OGCS}\boldsymbol{q}^t_{\mathcal{S}_{\forall-e}}\right)^* \otimes {}^{OGCS}\boldsymbol{q}^t_{\mathcal{S}_{\forall-r}} \\ &= {}_{Calib_\forall}\boldsymbol{\delta q} \otimes \left({}^{OGCS}\boldsymbol{q}^t_{\mathcal{S}_{\forall-r}}\right)^* \otimes {}_{OriEst_\forall}\boldsymbol{\delta q}^t \otimes {}^{OGCS}\boldsymbol{q}^t_{\mathcal{S}_{\forall-r}} \end{aligned} \tag{7}$$

Despite the explicitness in coordinate transformations' derivation, the algebraic value of quaternions are usually found hard to understand. Therefore, rotation vectors are employed in representing errors, as they also have better properties for linear approximation. Rotation vectors express the rotation axis and angle between two coordinate systems using a 3D vector [36]. Additionally, when the magnitude is small, the XYZ components of the rotation vector can be approximated as the XYZ angles of Euler angles [37], helping to understand the physical significance of the computed errors.

Given the small error magnitude, the rotation vector of segment orientation in (7) can be approximated as a linear combination of the rotation vectors associated with the two key error factors, see (8). Similarly, the joint rotation error is approximated as the linear combination of the rotation vectors associated with two segment orientation errors (see (9)), by substituting (6) into (5). The approximation can be proved

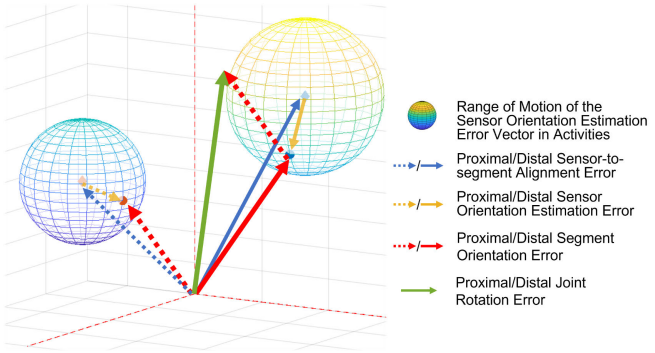

Fig. 3. Composition of sensor-to-segment alignment errors and IMU orientation estimation errors of proximal (thorax) and distal (upper arm) segments. The solid line represents the error vectors of the distal segment, and the dashed line represents the proximal segment errors. The sphere represents the range of endpoints of a fixed-magnitude sensor orientation estimation error vector across different segment orientations.

by converting quaternion representation into rotation matrices and linearly approximating the error matrices as the sum of the identity matrix and a skew-symmetric matrix [37], [38].

$${}^{\mathcal{S}_{\forall-e}}\boldsymbol{\delta\phi}^t_{\mathcal{S}_{\forall-r}} \approx {}_{Calib_\forall}\boldsymbol{\delta\phi} + \left({}^{OGCS}\boldsymbol{R}^t_{\mathcal{S}_{\forall-r}}\right)^{\mathsf{T}} \times {}_{OriEst_\forall}\boldsymbol{\delta\phi}^t \tag{8}$$

$${}_{JA}\boldsymbol{\delta\phi}^t \approx \left({}_{JA-r}\boldsymbol{R}^t\right)^{\mathsf{T}} \times {}^{\mathcal{S}_{T-e}}\boldsymbol{\delta\phi}^t_{\mathcal{S}_{\forall-r}} + {}^{\mathcal{S}_{T-e}}\boldsymbol{\delta\phi}^t_{\mathcal{S}_{\forall-r}} \tag{9}$$

where $\boldsymbol{R}$ denotes the rotation matrix that applied equivalent rotation on $\boldsymbol{\phi}$ with the quaternion multiplication ($\boldsymbol{q} \otimes [0, \boldsymbol{\phi}] \otimes \boldsymbol{q}^*$) applied. By substituting (8) into (9), the relationship between the joint rotation error and the two key error factors can be expressed as follows,

$$\begin{aligned} {}_{JA}\boldsymbol{\delta\phi}^t \approx{}& \left({}_{JA-r}\boldsymbol{R}^t\right)^{\mathsf{T}} \times {}_{Calib_T}\boldsymbol{\delta\phi} - {}_{Calib_U}\boldsymbol{\delta\phi} \\ &+ \left({}^{OGCS}\boldsymbol{R}^t_{\mathcal{S}_{U-r}}\right)^{\mathsf{T}} \times \left({}_{OriEst_T}\boldsymbol{\delta\phi}^t - {}_{OriEst_U}\boldsymbol{\delta\phi}^t\right) \end{aligned} \tag{10}$$

where the rotation matrices $\boldsymbol{R}$ only apply rotations to key error factors vectors without altering their magnitudes, defining the range of motion sphere for a fixed-magnitude error vector (Fig. 3). The overall shoulder joint error is the linear combination of rotation vectors representing sensor-to-segment alignment errors and orientation estimation errors on thorax and upper arm (see (10)). Two key error vectors, namely sensor-to-segment alignment error, and sensor orientation estimation error, from each segment first compose to the segment orientation error vector, which has an endpoint on a sphere centered at the endpoint of the sensor-to-segment alignment error vector (see (8)). Importantly, during the experiment, any change in sensor orientation estimation error magnitude will result in a deviation of the vector from its original sphere. Finally, the proximal and distal segment orientation error vectors are rotated and composited to form the joint rotation error vector (see (9)).

C. Quantifying Effect of Error Factors on Shoulder Rotation Error by Partial Derivative

As the shoulder rotation error can be approximated as the sum of four rotation vectors, the quantification of the

effects of error factors from two adjacent segments on the shoulder rotation error magnitude can be conducted through partial derivative. Expressed as a rotation vector, the shoulder rotation error's magnitude represents the axis-angle error in estimated shoulder rotation. The quantified effects, also referred to as the "effect Jacobian", are presented in (11) and (12).

$$\boldsymbol{J}^t = \begin{bmatrix} \frac{\partial \|{}_{JA}\boldsymbol{\delta\phi}^t\|}{\partial {}_{Calib_T}\boldsymbol{\delta x}} & \frac{\partial \|{}_{JA}\boldsymbol{\delta\phi}^t\|}{\partial {}_{Calib_U}\boldsymbol{\delta x}} & \frac{\partial \|{}_{JA}\boldsymbol{\delta\phi}^t\|}{\partial {}_{OriEst_T}\boldsymbol{\delta x}^t} & \frac{\partial \|{}_{JA}\boldsymbol{\delta\phi}^t\|}{\partial {}_{OriEst_U}\boldsymbol{\delta x}^t} \\ \frac{\partial \|{}_{JA}\boldsymbol{\delta\phi}^t\|}{\partial {}_{Calib_T}\boldsymbol{\delta y}} & \cdots & \cdots & \vdots \\ \frac{\partial \|{}_{JA}\boldsymbol{\delta\phi}^t\|}{\partial {}_{Calib_T}\boldsymbol{\delta z}} & \cdots & \cdots & \frac{\partial \|{}_{JA}\boldsymbol{\delta\phi}^t\|}{\partial {}_{OriEst_U}\boldsymbol{\delta x}^t} \end{bmatrix}$$

$$= \begin{bmatrix} \frac{{}_{JA}\boldsymbol{\delta x}^t}{\|{}_{JA}\boldsymbol{\delta\phi}^t\|} & & \\ & \frac{{}_{JA}\boldsymbol{\delta y}^t}{\|{}_{JA}\boldsymbol{\delta\phi}^t\|} & \\ & & \frac{{}_{JA}\boldsymbol{\delta z}^t}{\|{}_{JA}\boldsymbol{\delta\phi}^t\|} \end{bmatrix} \times \begin{bmatrix} {}_{Calib_T}\boldsymbol{K}^t \\ {}_{Calib_U}\boldsymbol{K}^t \\ {}_{OriEst_T}\boldsymbol{K}^t \\ {}_{OriEst_U}\boldsymbol{K}^t \end{bmatrix}^{\mathsf{T}}$$

$${}_{JA}\boldsymbol{\delta\phi}^t = \begin{bmatrix} {}_{JA}\boldsymbol{\delta x}^t & {}_{JA}\boldsymbol{\delta y}^t & {}_{JA}\boldsymbol{\delta z}^t \end{bmatrix},$$

$${}_{Calib_T}\boldsymbol{K}^t = \begin{bmatrix} \left[{}_{JA-r}\boldsymbol{R}^t\right]_{11} \\ \left[{}_{JA-r}\boldsymbol{R}^t\right]_{22} \\ \left[{}_{JA-r}\boldsymbol{R}^t\right]_{33} \end{bmatrix}^{\mathsf{T}},$$

$${}_{Calib_U}\boldsymbol{K}^t = \begin{bmatrix} -1 \\ -1 \\ -1 \end{bmatrix}^{\mathsf{T}}, \; {}_{OriEst_T}\boldsymbol{K}^t = -{}_{OriEst_U}\boldsymbol{K}^t \tag{11}$$

$${}_{OriEst_T}\boldsymbol{K}^t = \begin{bmatrix} \left[{}_{OGCS}\boldsymbol{R}^t_{\mathcal{S}_{U-r}}\right]_{11} \\ \left[{}_{OGCS}\boldsymbol{R}^t_{\mathcal{S}_{U-r}}\right]_{22} \\ \left[{}_{OGCS}\boldsymbol{R}^t_{\mathcal{S}_{U-r}}\right]_{33} \end{bmatrix}^{\mathsf{T}} \tag{12}$$

where $\boldsymbol{\delta x}, \boldsymbol{\delta y}, \boldsymbol{\delta z}$ denote the x, y, z component of the rotation vector $\boldsymbol{\delta\phi}$, respectively; $\left[\boldsymbol{R}^t\right]_{ij}$ denotes the value in the i row and j column of the corresponding rotation matrix $\boldsymbol{R}$; $\boldsymbol{J}^t$ denotes the "effect Jacobian" of the error factors'(one for each column) components at time t. Each element of the "effect Jacobian" represents the change in the magnitude of the shoulder rotation error resulting from a small variation in each error factor component. K denotes the coefficient in (11). Specifically, XYZ components of ${}_{Calib_T}K^t$ denotes the coefficients of respective XYZ components of ${}_{Calib_T}\boldsymbol{\delta x}^t$.

The mean shoulder rotation error of a trial is determined by averaging the error magnitudes at each time point throughout the trial. Additionally, since the shoulder rotation magnitudes at different time steps are independent of each other in calculation, the mean "effect Jacobian," $\overline{\boldsymbol{J}}$, which reflects the impact of error factor variations on the mean shoulder rotation error magnitude, can be computed as the average of the "effect Jacobian" values at each time point throughout the trial, as follows,

$$\overline{\|{}_{JA}\boldsymbol{\delta\phi}\|} = \textstyle\sum \|{}_{JA}\boldsymbol{\delta\phi}^t\| / \sum_t, \quad \overline{\boldsymbol{J}} = \textstyle\sum \boldsymbol{J}^t / \sum_t \tag{13}$$

III. Experiments and Results

A. Experimental Setup

Twenty five healthy subjects (age: 22.88 ± 0.86; height: 1.73 ± 0.07m; weight: 61.04 ± 9.21kg; gender: 17 males and 8 females; all right-handed) participated in this study. This experiment was performed in accordance with the Helsinki Declaration and was approved by the ethics committee of Shanghai Jiao Tong University (No. E2021013P). Ten reflective markers were placed on the anatomical bony landmarks for segment definition: sternum jugular notch (SJN), 7th cervical vertebra (CV7), midpoint between the inferior angles of most Caudal points of the two scapula (MAI), 1st thoracic vertebra (TV1), left/right lateral epicondyle of humerus (LHLE/RHLE), left/right medial epicondyle of humerus (LMLE/RMLE) and left/right acromion (LAC/RAC) (Fig. 1(b)). Carbon fiber plates with three reflective markers were manually aligned with IMUs mounted on the arms and thorax. These triple marker sets were used for OMC segment tracking. Five IMUs (MTw, Xsens Technologies, Netherlands) were strapped to left/right forearms, left/right upper arms, plevis and thorax of the subject, respectively. Specifically, to minimize the impact of soft tissue and mitigate occlusion of optical marker points, the upper arm IMUs were positioned on the lateral side near the elbow, without affecting elbow flexion. Forearm IMUs were positioned on the dorsal side near the back of the hand. The thorax IMU was positioned slightly below the MAI with a strap covering its top (not shown in Fig. 1(b)). The pelvis IMU was positioned at the midpoint between the left and right Ilium Posterior Superior (LIPS and RIPS) on the back of the pelvis to ensure a stable determination of the subject's facing direction during calibration. Since joint rotation/quaternion is estimated from the segment CS after calibration, there were no specific orientation requirements for IMU placement, as long as they were securely attached to their respective segments. A thirteen-camera stereophotogrammetric system (Vicon, Oxford, UK) and Visual3D (C Motion, MD, USA) were used for tracking segment movements and calculating reference shoulder rotation. The IMUs and Vicon system were electronically synchronized through a cable, and both systems collected the data at 100Hz. The experiment was conducted in a laboratory environment without ferromagnetic disturbances, and potential sources of such disturbances, such as badminton rackets and golf clubs, were checked to ensure they were sufficiently distant from the IMUs to avoid significant interference during the experiment.

B. Experimental Procedure

Once the markers and IMUs had been worn properly, subjects were instructed to perform elbow flexion/extension with palm facing inward (medial) for functional calibration of upper arm medial-lateral axis. Following a 5-second static neutral pose (N-pose) at the beginning of each trial, subjects performed five 2-minute trials of sports activities, including yoga, golf, swimming, dance, and badminton. In yoga, subjects were asked to imitate the selected yoga movements including Dragon Pose, Phantom Chair Pose, Warrior II Pose, and

Warrior I Pose. Each pose was held for at least 8 seconds and was performed twice. In golf, subjects were taught to use a real golf club to simulate golf swing in three level of amplitudes and intensity, including the drives, iron shots and putts. In swimming, subjects were asked to perform their familiar swimming styles using upper limb while standing. All participants performed the breaststroke and some also performed freestyle. In dance, participants were instructed to perform fitness dance movements, including certain Zumba actions such as side jumps with arm swings and hip rotations. In badminton, subjects were asked to perform familiar actions using a badminton racket, including smashes and drop shots.

C. Inertial and Optical Motion Capture Data Processing

Since the proposed model is not dependent on a specific side of the body, we applied the model to estimate right shoulder rotation for validation and discussion.

Following the CAST procedure [29], OMC-estimated reference segment CSs are determined through two steps: 1) calibrating the assumed constant transformation, ${}^{\mathcal{T}_{\forall-r}}\boldsymbol{q}_{\mathcal{S}_{\forall-r}}$, between the marker cluster local CS (referred to as the technical frame in CAST) and the segment's anatomical frame during the N-pose, and 2) tracking the movement of the marker cluster local CS, ${}^{OGCS}\boldsymbol{q}^{t}_{\mathcal{T}_{\forall-r}}$, (see (14)). Finally, the reference shoulder rotation is calculated as the relative orientation between the reference thorax CS and the reference upper arm CS. Both IMC- and OMC-estimated sensor-to-segment alignment is calibrated by combining static and functional calibration methods. Specifically, the axes of the OMC anatomical frames are defined using markers placed on anatomical landmarks [21], [39], except for the medial-lateral axis of the upper arm. This axis is defined as the elbow flexion axis during elbow flexion-extension [40]. The segment CSs for IMC are calibrated according to Table.II, following the prior research [13], [23]. The IMU orientation is obtained using a complementary filter [41], chosen for its low computational cost and relatively good accuracy performance. The marker cluster local CS are used for tracking segments in OMC and calculating reference IMU local CS by introducing an alignment transformation (see (15)). The transformation quaternion for each IMU local CS can be obtained from methods introduced in [33] and [34].

$$ {}^{OGCS}\boldsymbol{q}^{t}_{\mathcal{S}_{\forall-r}} = {}^{OGCS}\boldsymbol{q}^{t}_{\mathcal{T}_{\forall-r}} \otimes {}^{\mathcal{T}_{\forall-r}}\boldsymbol{q}_{\mathcal{S}_{\forall-r}} \tag{14} $$

$$ {}^{OGCS}\boldsymbol{q}^{t}_{\mathcal{I}_{\forall-r}} = {}^{OGCS}\boldsymbol{q}^{t}_{\mathcal{T}_{\forall-r}} \otimes {}^{\mathcal{T}_{\forall-r}}\boldsymbol{q}_{\mathcal{I}_{\forall-r}} \tag{15} $$

D. "Effect Jacobian" of Error Factors on Shoulder Rotation Error

The experimental data was analyzed using the proposed "effect Jacobian" to assess the impact of key error factors on the estimation error of shoulder joint rotation. Considering the tendency of the subjects' upper arms to incline during the N-pose and their potential for significant upper arm sensor-to-segment alignment error with a vertical assumption, the incline angle in the IMC calibration model (Table.II) was set to $\theta_{incline} = 5°$ for subsequent analysis and discussion.

TABLE II
ANATOMICAL SEGMENT CS DEFINITION FOR INERTIAL MOTION CAPTURE SYSTEM (RIGHT ARM)

Segment	Axes Definition
Thorax(T)	$\boldsymbol{Y_T} = {}^{IMU-T}Z_G/\|{}^{IMU-T}Z_G\|$:cranial
	$\boldsymbol{Z_T} = Y_T \wedge {}^{IMU-P}Z/\|Y_T \wedge {}^{IMU-P}Z\|$:lateral
	$\boldsymbol{X_T} = Z_T \wedge Y_T/\|Z_T \wedge Y_T\|$:anterior
Upper Arm(U)	$\boldsymbol{Z_U} = V_{Flex}/\|V_{Flex}\|$:lateral
	$\boldsymbol{X_U} = Z_U \wedge {}^{IMU-U}Z_G/\|Z_U \wedge {}^{IMU-U}Z_G\|$:anterior
	$\boldsymbol{Y_U} = X_U \wedge Z_U/\|X_U \wedge Z_U\|$:cranial
	Inclination: Rotate $\theta_{incline}$ around $-Z_U$

* For each segment, all axes vectors are expressed in IMU local CS of the segment. Z_G is the Z axis of IGCS assuming opposed to the gravity. ${}^{IMU-P}Z$ denotes the Z-axis of the pelvis IMU located on the back of the pelvis (Fig. 1(b)), with the negative direction -Z assumed to be the anatomical anterior. V_{Flex} is the elbow flexion-extension axis pointing lateral. θ_{inline} adjusts the inclination of the upper arm Y axis. Notably, increasing θ_{inline} leads to an increase in the Z component of the upper arm sensor-to-segment alignment error.

** IMU-T: IMU on thorax, IMU-P: IMU on pelvis, IMU-U: IMU on upper arm.

The mean magnitude of shoulder rotation errors were $8.13 \pm 3.50°$, $8.26 \pm 3.24°$, $9.03 \pm 3.63°$, $7.78 \pm 3.07°$, and $7.26 \pm 2.99°$ for yoga, golf, swimming, dance, and badminton, respectively (Fig. 4). The shoulder angle estimation error results can be equivalently represented as 'ZXY' Euler angle root mean square errors (RMSE), with average values of $6.4 \pm 3.5°$, $2.8 \pm 1.1°$, and $3.8 \pm 1.5°$ for extension/flexion, external/internal rotation, and adduction/abduction angles, respectively, across all trials. In addition, the mean magnitude of sensor-to-segment alignment errors (Factor A and B) was significantly larger (from 4.15° to 5.19°) than the orientation estimation errors (Factor C and D)(from 1.29° to 2.86°) ($p<0.05$). Among the components of the thorax sensor-to-segment alignment error (Factor A), the mean X component (ad/abduction) exhibited the smallest absolute value, ranging from $-0.63°$ to $-0.46°$, while the other two components did not show significant differences. In contrast, among the components of the upper arm sensor-to-segment alignment error (Factor B), the mean Z component (extension/flexion) showed the largest absolute value, with a negative value ranging from $-2.55°$ to $-1.79°$.

It is shown that the Z components of all error factors demonstrated larger absolute Jacobian values (from 0.29 to 0.45, from -0.62 to -0.53, from 0.12 to 0.36 and from

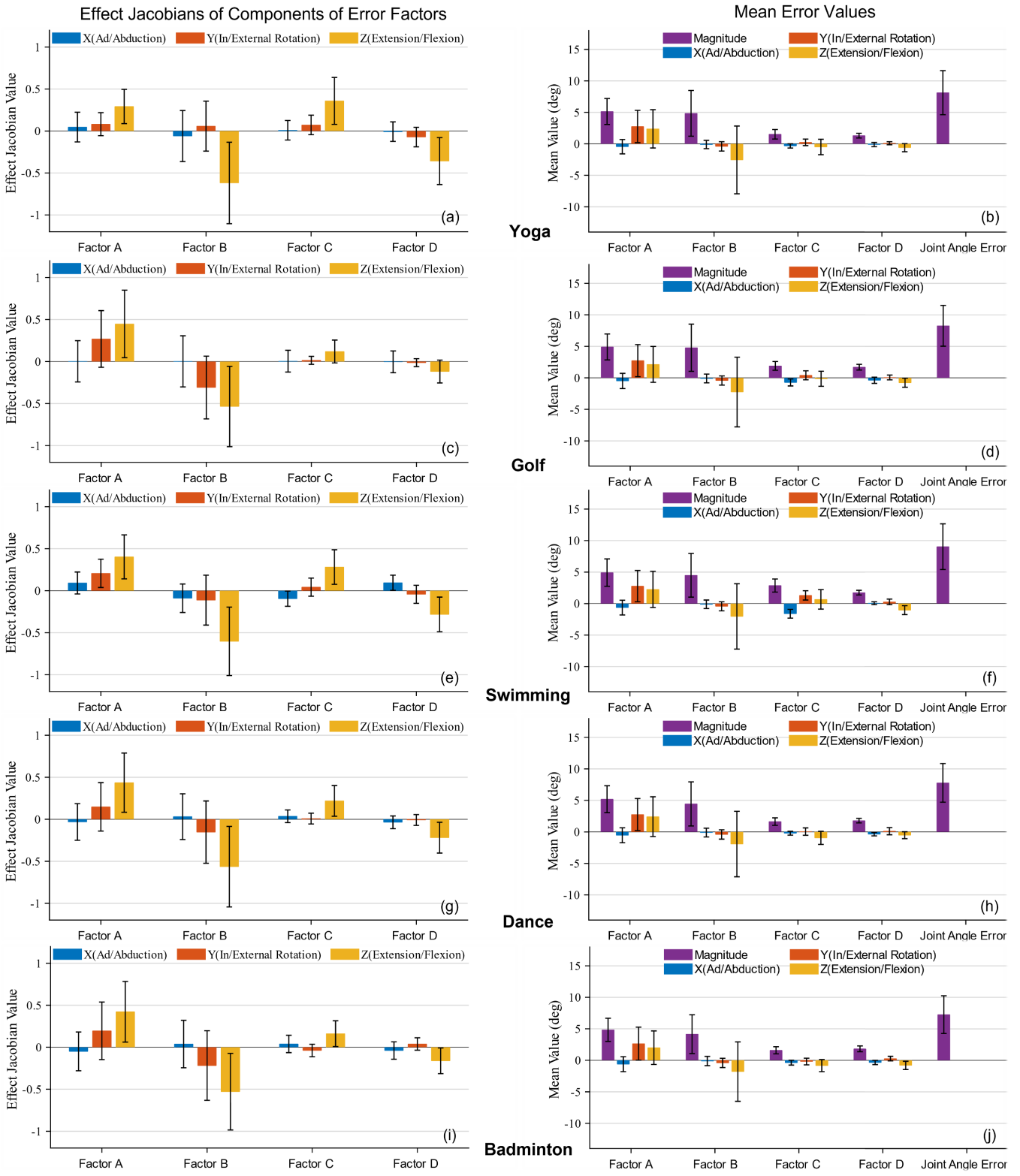

Fig. 4. The mean "effect Jacobian" values of Factor A,B,C, and D (left column) and the mean value of the error components and magnitude (right column) for five activities of all subjects' data when the upper arm incline angle $\theta_{incline} = 5°$ ($_{Calib_U}\delta z = -2.32$). The "effect Jacobian" measures the impact of a 1-unit change in the error factor component on the magnitude of the shoulder joint rotation error. The rows correspond to specific activities, namely yoga (a, b), golf (c, d), swimming (e, f), dance (g, h), and badminton (i, j). Factor A, B, C, and D represent key error factors related to the thorax and upper arm, specifically the thorax and upper arm sensor-to-segment alignment error, and the thorax and upper arm IMU orientation estimation error. The XYZ components of the error can be interpreted as the abduction/adduction $(+/-)$, internal/external rotation $(+/-)$, and extension/flexion $(+/-)$ in the sensor-to-segment alignment error. In the case of IMU orientation estimation error, the XYZ components correspond to the rotation around the XYZ axis in the *OGCS* (Z pointing vertically upward), respectively.

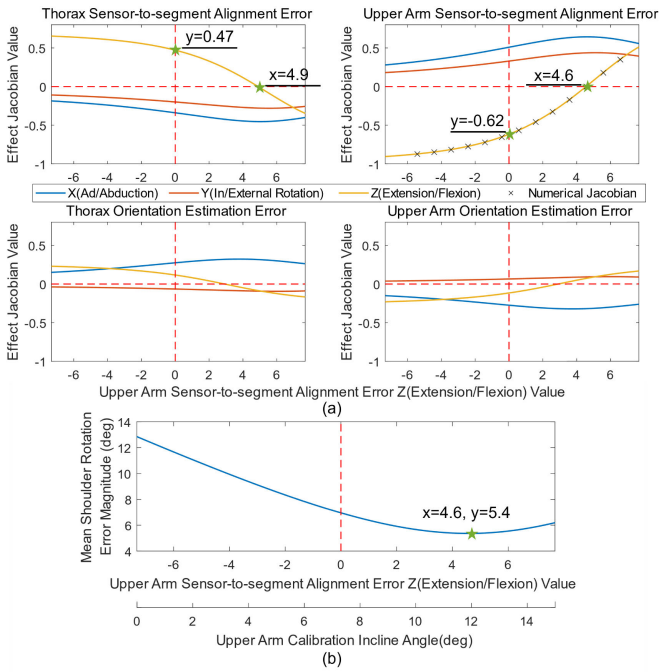

Fig. 5. Relationship between the Z component of upper arm sensor-to-segment alignment error and the "effect Jacobian" value (a) or mean shoulder rotation error magnitude (deg) (b) during a badminton trial conducted on one representative subject. The Z component of upper arm sensor-to-segment alignment error is manipulated by adjusting the assumed upper arm incline angle $\theta_{incline}$ from 0° to 15°(interior X axis value, specified in Table.II), corresponding to the superior X axis value changes from −7.3 to 7.7. Positive(+) and negative(−) alignment error values correspond to upper arm extension and flexion, respectively. The black cross indicates the numerical calculated Jacobian value at a specific point, obtained through differential calculation of shoulder rotation error with a step size of 0.1 degrees.

−0.36 to −0.12 for factor A, B, C, and D, respectively) compared to the other components ($p<0.05$) (Fig. 4). Specifically, the Z component of upper arm alignment error had a negative Jacobian value, consistent with its mean value. Notably, the thorax and upper arm orientation estimation errors (Factor C and D) exhibited opposite effects (Jacobian values) on the shoulder rotation error, which aligned with the derivations in (11) and (12).

The Jacobian coefficients, which were influenced by the reference shoulder rotation and upper arm orientation, exhibited variations among different activities. Specifically, there was no significant difference between golf and badminton activities ($p > 0.05$). However, a significant difference in the Jacobian values of the upper arm sensor-to-segment alignment error (factor B) Y component was observed between yoga and these two activities. In addition, the swimming activity showed a larger mean value (0.1 ± 0.13) in the Jacobian value of the X component of thorax sensor-to-segment alignment error compared to badminton and dance activities, indicating statistical significance.

Given the significant impact of the Z component of the upper arm alignment error on the magnitude of the shoulder rotation error, it was chosen as the independent variable for further investigation of the Jacobian value and overall error magnitude variation (Fig. 5). The numerically

TABLE III
MAXIMAL DIFFERENCE (DEG) BETWEEN LINEAR APPROXIMATED AND ANALYTICAL JOINT ROTATION ERRORS FOR FIVE SPORTS TRIALS - REPRESENTATIVE SUBJECT

	Yoga	Golf	Swimming	Dance	Badminton
Ad/Abduction	**0.45**	0.25	0.27	0.22	0.17
In/External Rotation	**0.37**	0.22	0.20	0.22	0.16
Extension/Flexion	0.08	0.16	**0.23**	0.17	0.18
Error Magnitude	0.07	0.05	**0.08**	0.03	0.03

The maximal values of approximation error in each dimension during five activities are highlighted.

calculated Jacobian value, obtained by calculating the differential $\Delta\|_{JA}\boldsymbol{\delta\phi}^t\|/\Delta_{Calib_U}\boldsymbol{\delta z}$, was expected to align with the curve reflecting the effect Jacobian values of upper arm sensor-to-segment misalignment. The effects of the error factor components on shoulder rotation error, as represented by effect Jacobian values, changed accordingly as the Z component of the upper arm alignment error varied from −7.3 to +7.7 (Fig. 5(a)). The upper arm alignment error was controlled by the upper arm incline angle, with the Z components of the alignment errors demonstrating the most significant change in the Jacobian values. Specifically, for the Z component of the upper arm sensor-to-segment alignment error, its effect became negligible (Jacobian value equals 0) when its error value reached 4.6. However, it continued to negatively impact the magnitude of the shoulder rotation error (Jacobian value equals −0.62) when the error value was 0. Additionally, the mean shoulder rotation error magnitude reached its lowest value of 5.4° when the upper arm alignment error was not at its smallest magnitude (Z component equals to 4.6) (Fig. 5).

E. Accuracy of Shoulder Rotation Error Linear Approximation

The proposed linear error approximation model demonstrates a high level of agreement with the analytically calculated shoulder rotation error across all five activities, validating its accuracy. The maximal differences between the linear approximation and analytical results are summarized in Table III. Specifically, the maximum differences in the X (ad/abduction), Y (in/external rotation), Z (extension/flexion) components, and error magnitude are measured as 0.33°, 0.27°, 0.17°, and 0.06°, respectively.

IV. DISCUSSION

This paper presents a novel linear approximation model to analyze the effect of two key error factors, namely sensor-to-segment alignment error and IMU orientation estimation error, on shoulder joint angle estimation. The model decouples and quantifies the effects of the two error factors on the magnitude of shoulder rotation errors, providing valuable insights for improving estimation accuracy. The results demonstrated that the proposed model was able to identify significant error components and determines adjustment strategies for post-hoc estimation accuracy improvement.

A. Shoulder Joint Estimation Accuracy

In this study, higher shoulder joint estimation accuracy was achieved compared to the previous studies involving shoulder angle estimation during movements with multiple degrees of freedom. For example, Truppa et al. [30] estimate upper limb kinematics during yoga and reported shoulder angle RMSE values of $3.2 \pm 1.0°$, $6.9 \pm 4.0°$, and $3.9 \pm 2.4°$ for extension/flexion, external/internal rotation, and adduction/abduction angles, respectively. Slade et al. [15] developed an IMC system for capturing full-body movements using an optimization algorithm. In their study on simulating knife cutting, the reported shoulder angle RMSEs were $6.9 \pm 4.2°$, $5.2 \pm 0.8°$, and $7.9 \pm 2.6°$. The observed improvement in accuracy in our study substantiates the effectiveness of introducing the incline angle in the calibration of the upper arm's longitudinal axis (Table. II). In addition, the Jacobian values demonstrate the potential for further enhancing shoulder angle estimation accuracy by increasing the incline angle. This is attributed to the significant negative effects of the Z component of the upper arm sensor-to-segment alignment error, which also exhibits a negative mean value, on the magnitude of the shoulder rotation error (Fig. 4). Increasing the incline angle leads to an increase in this Z component's value while reducing its magnitude, ultimately resulting in a decrease in the overall rotation error magnitude. The shoulder rotation error magnitude reaches its lowest point at an incline angle of 11.9° for this representative trial (Fig. 5(b)).

B. Effects of Error Factors on Shoulder Rotation Estimation Accuracy

By taking the partial derivative of the shoulder rotation error with respect to the error factor components, Jacobian values are derived to quantify the effects of sensor-to-segment misalignment and sensor orientation error. This approach differs from previous studies [18], [19], [42], which typically analyzed the effects of error factors by comparing the overall joint angle errors under limited predefined conditions, providing only a general understanding for other specific conditions. In contrast, the Jacobian values analytically indicate the change in joint rotation error magnitude resulting from a 1-unit improvement in any error factor component, specific to any experimental setup.

The analysis of Jacobian values revealed that improving the accuracy in the extension/flexion dimension of sensor-to-segment alignment error and IMU horizontal heading estimation (rotate around $OGCS$ Z axis, pointing vertically upward) had the most significant impact on enhancing shoulder angle estimation. Specifically, the Z component of the upper arm sensor-to-segment alignment error exhibited the largest absolute mean Jacobian value, approximately -0.5. From an experimental standpoint, these results suggest that making adjustments to the calibration assumption regarding the longitudinal axis inclination ($\theta_{incline}$) or instructing subjects to maintain a more upright posture for both the thorax and upper arm, thereby improving sensor-to-segment alignment error in the extension/flexion dimension, could yield the most significant enhancements in shoulder joint angle estimation accuracy within the context of our current experimental setup and sports activities. Furthermore, avoiding ferromagnetic disturbances or utilizing orientation algorithms with improved IMU heading estimation capabilities can also effectively enhance the shoulder angle estimation accuracy. The significant effects of error factor Z components may be attributed to the relatively large Z component of the shoulder rotation error itself, leading to a large Z coefficient in the diagonal matrix from (12). However, despite sharing the same coefficient with alignment error for each component, the impact of orientation estimation error is mitigated by the upper arm orientation-related coefficient $\boldsymbol{K}$ (Fig. 4). Additionally, the opposite impact of thorax and upper arm orientation estimation errors, as indicated by the Jacobian values and (13), suggests the possibility of partial error cancellation. This arises from the fact that the joint rotation/angles are calculated based on the relative orientation of the proximal and distal segments, and introducing the same orientation offset to both the proximal and distal segment tracking IMUs does not affect their relative orientation. However, the Jacobian value still captures the significance of the orientation estimation error component, considering that the errors of the two IMUs may not be exactly the same. Overall, the effectiveness of improving each error factor component is quantified by the Jacobian values, and our experiment demonstrates that enhancing thorax and upper arm calibration through the inclusion of extension/flexion in the calibration assumption or instructing subjects to perform a more upright posture is the most effective strategy for improving estimation accuracy.

Significant variations in error impact were observed across different activities, suggesting that the optimal strategy for accuracy improvement may differ depending on the specific joint range of motion required for each application. Minimal differences in error impact were observed between badminton and golf, while yoga and swimming exhibited substantial variations. These discrepancies can be attributed to the distinct joint pose distributions associated with each activity. In badminton and golf, the shoulder encompasses a wide range of motion, whereas breaststroke swimming primarily involves movements in the anterior region of the body, and yoga typically involves a limited set of poses. These findings underscore the importance of considering the activity-specific joint pose distribution when determining the most effective approach for enhancing estimation accuracy.

The Jacobian values can vary as the error factors improve. However, achieving the minimum shoulder rotation error is unlikely when the error factors are reduced to zero. This highlights the importance of analyzing the Jacobian values of the error factors. It can be observed that even when there is no error in the extension/flexion dimension of the upper arm sensor-to-segment misalignment, this component still has a negative effect on the shoulder rotation error magnitude (Fig. 5(a)). This finding suggests that further increasing the extension/flexion dimension of the upper arm sensor-to-segment alignment error could potentially lead to a reduction in the shoulder rotation error for this representative trial. Consequently, the optimal shoulder angle estimation accuracy is achieved when the upper arm sensor-to-segment alignment

error in the extension/flexion dimension is +4.6 (corresponding to an incline angle of 11.9°) (Fig. 5(b)). This phenomenon of over-correction is likely due to the potential cancellation of errors. Since the overall shoulder rotation error vector is composed of four error factor-related vectors (Fig. 3), it is natural that these error vectors can cancel each other out under specific joint poses. Therefore, over-correction has the potential to further decrease the shoulder rotation error magnitude, although its extent is dependent on the specific activity and requires analysis based on the Jacobian values.

C. Limitations

There remain several limitations to this study. First, our study did not account for soft tissue artifacts (STA) errors during the joint rotation estimation and error analytical model. STA is often excluded from motion capture algorithms, especially for IMC systems, due to the difficulty in obtaining the underlying bone orientation. However, incorporating STA errors into the error analytical model could enhance its applicability to motion capture systems that find it necessary to account for STA errors. Second, the effectiveness of each error component in reducing joint rotation error (Jacobian value) is specific to the current joint rotation estimation algorithm and data. Jacobian values may change when modifications are made to the algorithm, such as IMU orientation estimation, calibration assumptions, or the calibration protocol. To achieve a high level of accuracy, the proposed error decoupling model may need to be iteratively applied after accuracy improvement efforts until satisfactory results are obtained. Third, the method was validated on healthy subjects, and its potential application in shoulder capture rehabilitation systems for patients with conditions like stroke or Parkinson's disease has not been explored.

D. Future Work

In the future, research efforts should prioritize several key aspects. First, there is a need for further investigation into a robust method for quantifying STA errors and integrating these errors into the analytical error decoupling model. This will enable an analytical evaluation of its impact on joint rotation error. Such integration can make the analytical error decoupling model more comprehensive and applicable to various types of motion capture systems, thereby enhancing joint angle estimation accuracy across diverse applications. Second, the proposed linear approximation model and analytical error factor impact analysis were specifically implemented for shoulder angle estimation. Although the error definition and derivation presented in this paper are not joint-specific, the extension of the method to other joints would enhance its applicability and could serve as a foundation for analyzing joint moment error factors in the lower body. Third, as one of the major benefits of improving IMU-based motion capture accuracy is the enhancement of rehabilitation systems and the potential for home-based rehabilitation, future research efforts should concentrate on validating and guiding accuracy improvements in rehabilitation applications on patients. Such endeavors could have significant societal benefits by advancing the field of rehabilitation and making it more accessible to a wider range of individuals.

V. Conclusion

In this paper, we present a novel linear approximation model to decouple and analytically evaluate the effects of two key errors, namely sensor-to-segment misalignment and IMU orientation estimation error, on the IMC estimated shoulder angle estimation error. Our model successfully provide quantified insights (effect Jacobian) into the significance of each error factor component, demonstrating the consequential change in shoulder rotation error under a 1-unit improvement in the corresponding error factor. The validation of our linear approximation model on the experimental data comprising twenty-five subjects engaged in five different sports activities has shown satisfactory accuracy. The analysis of Jacobian values has revealed the substantial impact of improving the extension/flexion dimension of thorax and upper arm sensor-to-segment alignment, as well as the effectiveness of enhancing yaw estimation (rotation around the vertical axis) for improving shoulder angle estimation accuracy. This research holds the potential to guide the accuracy improvement of joint angle estimation in rehabilitation and sport performance evaluation, as this post-hoc analysis offers the opportunity to develop subject- or movement-specific models with high accuracy based on their experiment result. Additionally, our proposed linear approximation model of joint angle estimation error bridges the gap between error factors and joint rotation error through explicit linear composition.

References

[1] S. D. Skejø, M. Møller, J. Bencke, and H. Sørensen, "Shoulder kinematics and kinetics of team handball throwing: A scoping review," *Human Movement Sci.*, vol. 64, pp. 203–212, Apr. 2019.

[2] S. Namdari et al., "Defining functional shoulder range of motion for activities of daily living," *J. Shoulder Elbow Surgery*, vol. 21, no. 9, pp. 1177–1183, Sep. 2012.

[3] X. Song, S. Chen, J. Jia, and P. B. Shull, "Cellphone-based automated fugl-meyer assessment to evaluate upper extremity motor function after stroke," *IEEE Trans. Neural Syst. Rehabil. Eng.*, vol. 27, no. 10, pp. 2186–2195, Oct. 2019.

[4] L. Bai, M. G. Pepper, Y. Yan, S. K. Spurgeon, M. Sakel, and M. Phillips, "Quantitative assessment of upper limb motion in neurorehabilitation utilizing inertial sensors," *IEEE Trans. Neural Syst. Rehabil. Eng.*, vol. 23, no. 2, pp. 232–243, Mar. 2015.

[5] H. Zhou and G. Alici, "Non-invasive human-machine interface (HMI) systems with hybrid on-body sensors for controlling upper-limb prosthesis: A review," *IEEE Sensors J.*, vol. 22, no. 11, pp. 10292–10307, Jun. 2022.

[6] M. M. B. Morrow, B. Lowndes, E. Fortune, K. R. Kaufman, and M. S. Hallbeck, "Validation of inertial measurement units for upper body kinematics," *J. Appl. Biomechanics*, vol. 33, no. 3, pp. 227–232, Jun. 2017.

[7] B. Guignard et al., "Validity, reliability and accuracy of inertial measurement units (IMUs) to measure angles: Application in swimming," *Sports Biomechanics*, pp. 1–33, Jul. 2021.

[8] S. Qiu et al., "Sensor combination selection strategy for kayak cycle phase segmentation based on body sensor networks," *IEEE Internet Things J.*, vol. 9, no. 6, pp. 4190–4201, Mar. 2022.

[9] S. Rawashdeh, D. Rafeldt, and T. Uhl, "Wearable IMU for shoulder injury prevention in overhead sports," *Sensors*, vol. 16, no. 11, p. 1847, Nov. 2016.

[10] J. McGrath, J. Neville, T. Stewart, and J. Cronin, "Upper body activity classification using an inertial measurement unit in court and field-based sports: A systematic review," *Proc. Inst. Mech. Eng., P, J. Sports Eng. Technol.*, vol. 235, no. 2, pp. 83–95, Jun. 2021.

[11] A. Filippeschi, N. Schmitz, M. Miezal, G. Bleser, E. Ruffaldi, and D. Stricker, "Survey of motion tracking methods based on inertial sensors: A focus on upper limb human motion," *Sensors*, vol. 17, no. 6, p. 1257, Jun. 2017.

[12] U. G. Longo, S. De Salvatore, M. Sassi, A. Carnevale, G. De Luca, and V. Denaro, "Motion tracking algorithms based on wearable inertial sensor: A focus on shoulder," *Electronics*, vol. 11, no. 11, p. 1741, May 2022.

[13] A. G. Cutti, A. Giovanardi, L. Rocchi, A. Davalli, and R. Sacchetti, "Ambulatory measurement of shoulder and elbow kinematics through inertial and magnetic sensors," *Med. Biol. Eng. Comput.*, vol. 46, no. 2, pp. 169–178, 2008.

[14] Z.-Q. Zhang, W.-C. Wong, and J.-K. Wu, "Ubiquitous human upper-limb motion estimation using wearable sensors," *IEEE Trans. Inf. Technol. Biomed.*, vol. 15, no. 4, pp. 513–521, Jul. 2011.

[15] P. Slade, A. Habib, J. L. Hicks, and S. L. Delp, "An open-source and wearable system for measuring 3D human motion in real-time," *IEEE Trans. Biomed. Eng.*, vol. 69, no. 2, pp. 678–688, Feb. 2022.

[16] S. Qiu et al., "Sensor network oriented human motion capture via wearable intelligent system," *Int. J. Intell. Syst.*, vol. 37, no. 2, pp. 1646–1673, Feb. 2022.

[17] R. Pellois and O. Brüls, "An inertial human upper limb motion tracking method for robot programming by demonstration," *Robot. Auto. Syst.*, vol. 156, Oct. 2022, Art. no. 104201.

[18] K. Lebel, P. Boissy, H. Nguyen, and C. Duval, "Inertial measurement systems for segments and joints kinematics assessment: Towards an understanding of the variations in sensors accuracy," *Biomed. Eng. OnLine*, vol. 16, no. 1, pp. 1–16, Dec. 2017.

[19] B. Fan, Q. Li, T. Tan, P. Kang, and P. B. Shull, "Effects of IMU sensor-to-segment misalignment and orientation error on 3-D knee joint angle estimation," *IEEE Sensors J.*, vol. 22, no. 3, pp. 2543–2552, Feb. 2022.

[20] H. Kamstra, E. Wilmes, and F. C. T. van der Helm, "Quantification of error sources with inertial measurement units in sports," *Sensors*, vol. 22, no. 24, p. 9765, Dec. 2022.

[21] G. Wu et al., "ISB recommendation on definitions of joint coordinate systems of various joints for the reporting of human joint motion—Part II: Shoulder, elbow, wrist and hand," *J. Biomechanics*, vol. 38, no. 5, pp. 981–992, May 2005.

[22] R. V. Vitali and N. C. Perkins, "Determining anatomical frames via inertial motion capture: A survey of methods," *J. Biomechanics*, vol. 106, Jun. 2020, Art. no. 109832.

[23] W. H. K. de Vries, H. E. J. Veeger, A. G. Cutti, C. Baten, and F. C. T. van der Helm, "Functionally interpretable local coordinate systems for the upper extremity using inertial & magnetic measurement systems," *J. Biomechanics*, vol. 43, no. 10, pp. 1983–1988, Jul. 2010.

[24] A. Carnevale et al., "Wearable systems for shoulder kinematics assessment: A systematic review," *BMC Musculoskeletal Disorders*, vol. 20, no. 1, pp. 1–24, Dec. 2019.

[25] B. Fan, H. Xia, J. Xu, Q. Li, and P. B. Shull, "IMU-based knee flexion, abduction and internal rotation estimation during drop landing and cutting tasks," *J. Biomechanics*, vol. 124, Jul. 2021, Art. no. 110549.

[26] M. Nazarahari and H. Rouhani, "Sensor fusion algorithms for orientation tracking via magnetic and inertial measurement units: An experimental comparison survey," *Inf. Fusion*, vol. 76, pp. 8–23, Dec. 2021.

[27] P. Picerno et al., "Upper limb joint kinematics using wearable magnetic and inertial measurement units: An anatomical calibration procedure based on bony landmark identification," *Sci. Rep.*, vol. 9, no. 1, p. 14449, Oct. 2019.

[28] S. Cai, M. Shao, M. Du, G. Bao, and B. Fan, "A binocular-camera-assisted sensor-to-segment alignment method for inertial sensor-based human gait analysis," *IEEE Sensors J.*, vol. 23, no. 3, pp. 2663–2671, Feb. 2023.

[29] A. Cappozzo, F. Catani, U. Della Croce, and A. Leardini, "Position and orientation in space of bones during movement: Anatomical frame definition and determination," *Clin. Biomechanics*, vol. 10, no. 4, pp. 171–178, Jun. 1995.

[30] L. Truppa, E. Bergamini, P. Garofalo, G. Vannozzi, A. M. Sabatini, and A. Mannini, "Magnetic-free quaternion-based robust unscented Kalman filter for upper limb kinematic analysis," *IEEE Sensors J.*, vol. 23, no. 3, pp. 3212–3219, Feb. 2023.

[31] H. J. Luinge, P. H. Veltink, and C. T. M. Baten, "Ambulatory measurement of arm orientation," *J. Biomechanics*, vol. 40, no. 1, pp. 78–85, Jan. 2007.

[32] P. Müller, M.-A. Bégin, T. Schauer, and T. Seel, "Alignment-free, self-calibrating elbow angles measurement using inertial sensors," *IEEE J. Biomed. Health Informat.*, vol. 21, no. 2, pp. 312–319, Mar. 2017.

[33] H. Mecheri, X. Robert-Lachaine, C. Larue, and A. Plamondon, "Evaluation of eight methods for aligning orientation of two coordinate systems," *J. Biomechanical Eng.*, vol. 138, no. 8, Aug. 2016, Art. no. 084501.

[34] W. H. K. de Vries, H. E. J. Veeger, C. T. M. Baten, and F. C. T. van der Helm, "Magnetic distortion in motion labs, implications for validating inertial magnetic sensors," *Gait Posture*, vol. 29, no. 4, pp. 535–541, Jun. 2009.

[35] P. Picerno, A. Cereatti, and A. Cappozzo, "A spot check for assessing static orientation consistency of inertial and magnetic sensing units," *Gait Posture*, vol. 33, no. 3, pp. 373–378, Mar. 2011.

[36] J. Diebel, "Representing attitude: Euler angles, unit quaternions, and rotation vectors," *Matrix*, vol. 58, nos. 15–16, pp. 1–35, 2006.

[37] H. J. Woltring, R. Huiskes, A. de Lange, and F. E. Veldpaus, "Finite centroid and helical axis estimation from noisy landmark measurements in the study of human joint kinematics," *J. Biomechanics*, vol. 18, no. 5, pp. 379–389, Jan. 1985.

[38] A. Brennan, K. Deluzio, and Q. Li, "Assessment of anatomical frame variation effect on joint angles: A linear perturbation approach," *J. Biomechanics*, vol. 44, no. 16, pp. 2838–2842, Nov. 2011.

[39] G. Rab, K. Petuskey, and A. Bagley, "A method for determination of upper extremity kinematics," *Gait Posture*, vol. 15, no. 2, pp. 113–119, Apr. 2002.

[40] F. Fraysse and D. Thewlis, "Comparison of anatomical, functional and regression methods for estimating the rotation axes of the forearm," *J. Biomechanics*, vol. 47, no. 14, pp. 3488–3493, Nov. 2014.

[41] B. Fan, Q. Li, and T. Liu, "Improving the accuracy of wearable sensor orientation using a two-step complementary filter with state machine-based adaptive strategy," *Meas. Sci. Technol.*, vol. 29, no. 11, Nov. 2018, Art. no. 115104.

[42] C. Jiang, Y. Yang, H. Mao, D. Yang, and W. Wang, "Effects of dynamic IMU-to-segment misalignment error on 3-DOF knee angle estimation in walking and running," *Sensors*, vol. 22, no. 22, p. 9009, Nov. 2022.